GA–A26761

TOROIDALLY RESOLVED STRUCTURE OF DIVERTOR HEAT FLUX IN RMP H-MODE DISCHARGES ON DIII-D

by

M.W. JAKUBOWSKI, T.E. EVANS, M.E. FENSTERMACHER, C.J. LASNIER, O. SCHMITZ, R.C. WOLF, L.R. BAYLOR, J.A. BOEDO, K.H. BURRELL, J.S. deGRASSIE, P. GOHIL, S. MORDIJCK, R. LAENGNER, A.W. LEONARD, R.A. MOYER, T.W. PETRIE, C.C. PETTY, R.I. PINSKER, T.L. RHODES, M.J. SCHAFFER, P.B. SNYDER, H. STOSCHUS, T.H. OSBORNE, D.M. ORLOV, E.A. UNTERBERG, and J.G. WATKINS

JULY 2010

GENERAL ATOMICS

DISCLAIMER

GA–A26761

TOROIDALLY RESOLVED STRUCTURE OF DIVERTOR HEAT FLUX IN RMP H-MODE DISCHARGES ON DIII-D

by
M.W. JAKUBOWSKI,* T.E. EVANS, M.E. FENSTERMACHER,† C.J. LASNIER,† O. SCHMITZ,‡ R.C. WOLF,* L.R. BAYLOR,¶ J.A. BOEDO,§ K.H. BURRELL, J.S. deGRASSIE, P. GOHIL, S. MORDIJCK,§ R. LAENGNER,‡ A.W. LEONARD, R.A. MOYER,§ T.W. PETRIE, C.C. PETTY, R.I. PINSKER, T.L. RHODES,# M.J. SCHAFFER, P.B. SNYDER, H. STOSCHUS,‡ T. OSBORNE, D.M. ORLOV,§ E.A. UNTERBERG,¶ and J.G. WATKINS◊

This is a preprint of a paper to be presented at the Nineteenth International Conference on Plasma Surface Interactions, May 24-28, 2010, in San Diego, California, and to be published in the *Proceedings.*

*Max-Planck-Institut für Plasmaphysik, IPP-EURATOM Association, Greifswald, Germany,
†Lawrence Livermore National Laboratory, Livermore, California.
‡Forschungszentrum Jülich, IEF-4, Association FZJ-EURATOM, TEC, Jülich, Germany.
¶Oak Ridge National Laboratory, Oak Ridge, Tennessee.
§University of California-San Diego, La Jolla, California.
#University of California-Los Angeles, Los Angeles, California.
◊Sandia National Laboratories, Albuquerque, New Mexico.

Work supported in part by
the U.S. Department of Energy
under DE-FC02-04ER54698, DE-AC52-07NA27344,
DE-AC05-00OR22725, DE-FG02-08ER54984,
DE-FG02-07ER54917, and DE-AC04-94AL85000

GENERAL ATOMICS ATOMICS PROJECT 30200
JULY 2010

GENERAL ATOMICS

ABSTRACT

As shown on DIII-D edge localized modes (ELMs) can be either completely eliminated or mitigated with resonant magnetic perturbation fields. Application of Resonant Magnetic Perturbation (RMP) fields results in a 3D magnetic topology that affects heat loads for ELM-suppressed discharges as well as the smaller ELMs seen during mitigated scenarios. Two infrared cameras, separated 105 deg toroidally, were used to make simultaneous measurements of ELM heat loads with high frame rates. Without the RMP fields ELMs display a variety of different heat load dynamics and a range of toroidal variability that is characteristic of their 3D structure. Comparing radial averages there is no asymmetry between two toroidal locations. With RMP mitigated ELMS, the variability in the radially averaged power loads is significantly reduced even though toroidal asymmetries in power loads are introduced. In addition to RMP ELM suppression scenarios an RMP scenario with only very small ELMs has been achieved.

I. INTRODUCTION

It is assumed that the next step fusion devices, such as ITER, will operate in regimes with high-energy confinement in order to demonstrate good rate of fusion power production. The discharge scenario that fulfils those requirements is so-called H-mode [1]. An undesirable consequence of the high confinement is periodic formation of large transient power loads to the plasma facing components due to type-I edge localized mode (ELM) events [2,3]. In recent years, clear evidence of the ELM as a filamentary structure [4,5] propagating radially across the scrape-off layer (SOL) and extending far outside the separatrix [6,7] has been developed. ELMs also form characteristic patterns on the divertor surface, where several discrete substructures have been measured on ASDEX Upgrade [8] and recently also on DIII-D [9]. The power loads due to type-I ELMs are of great concern for lifetime and durability of the divertors in future devices like ITER [10]. Therefore, extensive studies of the heat distribution on the plasma facing components are performed in tokamaks. Typically it is assumed that there is toroidal symmetry of heat loads and the structure of strike lines [3,11] on the divertor surface. On the other hand, there are also recent studies [12], which suggest that thermo-electric currents flowing within the filaments form three-dimensional structures of ELM deposition patterns that are not toroidally symmetric. In principle any finite n instability that results in heat bursts should create 3D structures.

As shown on DIII-D, type-I ELMs can be either completely eliminated [13,14] or mitigated with Resonant Magnetic Perturbation (RMP) fields, which stochastically open edge field lines to the divertor [15,16]. This is a very promising scenario for ITER, as it enhances significantly the survival of the plasma facing components material.

In this work we study the validity of the assumption of toroidal symmetry of ELM heat loads to the divertor on DIII-D and how this is affected by application of the magnetic perturbations. Here, we show that it is possible to achieve a regime where very small regular ELMs appear with deposition patterns following topology of stochastic boundary. The amplitude and toroidal distribution of heat loads in this regime are sensitive to q_{95}.

II. EXPERIMENTAL SETUP

Previous studies of RMP effects on ELMs in DIII-D have been performed with ITER-similar shape and with ITER-like electron pedestal collisionality [9]. That configuration was unfavorable for the observation of the outer leg, which was partially covered by the pump duct. Therefore in this work the plasma shape has been optimized for the infra-red systems, i.e. the outer leg has been pulled out from the pump duct on top of the pump duct shelf, which resulted in average plasma triangularity about 0.3 and electron pedestal collisionality of $\nu^* \approx 1$. Important plasma parameters have been presented in Fig. 1. The analysis is based on four discharges with all parameters identical except q_{95}, which was varied from 3.5 to 4.3, in order to scan the resonant window of interaction between RMPs and the plasma magnetic equilibrium. The heat flux density was measured with two infrared cameras separated toroidally by $\Delta\varphi = 105$ deg. At $\varphi = 60$ deg a FLIR SC6000 camera with spatial resolution of about 6-7 mm and frame rate of 12 kHz was used and at $\varphi = 165$ deg was an SBF-125 camera with spatial resolution of 9-10 mm and frame rate of 13 kHz was used. Both cameras observed the lower divertor floor through similar optical elements. An absolute calibration of both IR systems was performed during the same machine bake in order to assure consistent calibration curves. The heat fluxes on the target surfaces are calculated by applying a standard numerical solution of the two-dimensional heat diffusion equations to the evolution of the surface temperature on the investigated area with the THEODOR code [17]. The code, which is used to study heat loads due to type-I ELMs, has the ability to evaluate the influence of the surface layers on the evaluated heat flux density. THEODOR starts from the temporal evolution of the surface temperature distribution along the poloidal target coordinate and computes the heat flux distribution using a 2D slab geometry approximation for the target tiles, introducing the real poloidal target width and an averaged target thickness. Front surface layers are taken into account with the heat transmission coefficient α, which is chosen in such a way that negative heat fluxes in the inter-ELM period are avoided. The coefficient assumes the same surface properties across the divertor strike line, which is not necessarily correct; therefore, some caution must be taken with absolute numbers of the heat flux density. A detailed discussion of the method and examples of ASDEX-Upgrade and JET data are given in [17,18]. In this work the choice of α coefficient was rather critical as we perform comparison of both camera data at two different toroidal locations. One of the main criteria is how the heat flux behaves in the decay phase. We have assumed, following [17,18], that negative values would be unphysical. We have set α always to the highest possible value possible, such that power flux q (MW) did not become negative. Typical values for inner leg are 100 $\left(\text{kW m}^{-2}\text{ K}^{-1}\right)$ at $\varphi = 60$ deg and

40 $\left(\mathrm{kW\ m^{-2}\ K^{-1}}\right)$ at $\varphi = 165$ deg and 65–70 $\left(\mathrm{kW\ m^{-2}\ K^{-1}}\right)$ for the outer leg at both locations. Since the evaluated time behavior of the heat flux density at the strike point during an ELM is much more sensitive than energy integrated over time to the choice of α then the energy integrated over time, we have decided to calculate toroidal asymmetries during ELMs from the total energy lost during an ELM rather than heat flux density.

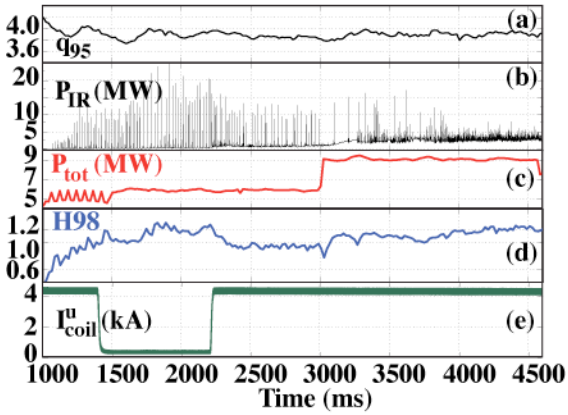

Fig. 1: Overview of main plasma parameters for the discharge #139745 – from top: (a) safety factor at ψ_{95} (q_{95}), (b) power to the inner divertor evaluated from IR data (P_{IR}), (c) H98 factor, (d) total heating power (P_{tot}) and (e) current amplitude in RMP coils (I-coil).

The investigated discharges were divided into four different phases (see Fig. 1).

1. Initial RMP phase (t < 1500 ms), in which we have tried to see to what extent one can control ELMs with magnetic perturbation turned on before onset of the H-mode.
2. Very small RMP phase (1500 ms < t < 2200 ms) with very low level of I-coil current (below 1 kA) as a reference case for the time with RMP turned on.
3. Phase with RMP and 6 MW of total heating power (2200 ms < t 3000 ms), to study the influence of stochastic boundary on ELMs with magnetic perturbation applied during an H-mode.
4. Phase with RMP and 9 MW of total heating power (t > 3000 ms). The higher heating power was established to study beta effects on penetration of magnetic perturbation field.

III. EXPERIMENTAL RESULTS

An example of results for one of the investigated discharges (#139745, q_{95} = 3.9) is shown in Fig. 1. In the initial phase (t < 1500 ms) I-coil currents reduce size of power loads by factor of 2 as compared to non-RMP phase, which starts at t = 1500 ms. Where Switching on the magnetic perturbations at t = 2200 ms reduces amplitudes of ELMs by factor of 2 with frequency increasing by factor of 2 as well. At the same time H98 drops slightly below 1. As will be shown later, the effect of the RMP on ELMs strongly depends on the value of q_{95}. Increasing heating power to 9 MW at t = 3000 ms results in increase of H98 to pre-RMP value and at the same time reduces ELMs; their amplitude is smaller by almost a factor of 5 as compared to the non-RMP phase as compared to the non-RMP phase. This is a rather robust effect for all discharges; higher heating power results in better coupling of the magnetic perturbation with the plasma magnetic equilibrium. This seems to be in contradiction to present theories on penetration of external fields [19]. These theories would predict that higher plasma rotation and pedestal temperature should help screen penetration more effectively. Also one needs to remember that higher heating power results in small change of equilibrium.

In Fig. 2 parameters characterizing ELMs in different stages of each discharge of q_{95} are presented. Quantities presented there are averaged over all events in a given phase with error bars showing the standard deviation. This gives an estimate of the variability for a given parameter. Two different parameters are shown as a function of q_{95} (the abscissa): 1) mean energy deposited to the lower divertor (sum of inner and outer leg) averaged over both toroidal locations [E (kJ)], and toroidal asymmetry between deposited energy radially integrated measured at two toroidal locations (R). Blue squares show results for the non-RMP phase, red triangles for the time range (2300 < t < 3000 ms) with RMP and 6 MW of total heating power and green diamonds for the phase with RMP and 9 MW of heating power (3500 < t < 4200).

The average energy in the non-RMP phase almost does not change with q_{95} from slightly above 8 kJ at q_{95} = 3.5 to 7 kJ at q_{95} = 4.3 with standard deviation of order of 50%. Introducing RMP can significantly reduce average size of the ELMs as well as the variability of the deposited energy. The red curve shows reduction of E to 5 kJ at q_{95} = 3.5 with standard deviation of about 1 kJ; as the q_{95} increases the level of reduction is smaller. For q_{95} > 4.1 E has the same value as without magnetic perturbation. Nevertheless, the variability with RMP remains smaller than without RMP for all the cases investigated. Introducing higher heating power (green curve) makes the ELMs smaller as compared to the 6 MW case. There is no data point for q_{95} = 3.5 as

increasing the neutral beam injection triggered a tearing mode. At higher power we see a similar tendency, the average ELM size decreases to about 3 kJ at $q_{95} = 3.9$. The variability of the ELM size is smaller than in both the non-RMP case and smaller than the case with RMP and P_{tot} = 6 MW.

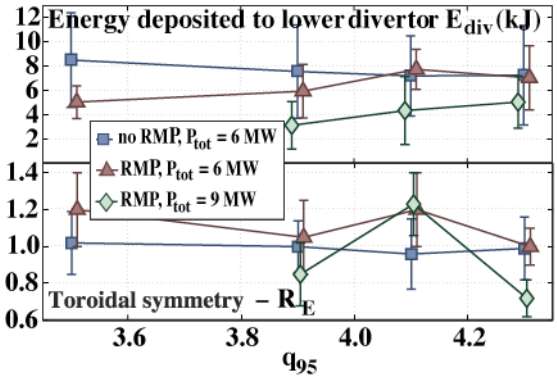

Fig. 2: Dependence of parameters characterizing heat loads to the inner leg of the lower divertor on q_{95} - from top: energy deposited to the divertor averaged over both toroidal locations, toroidal asymmetry between deposited energy measured by two cameras (R).

The lower graph in Fig. 2 shows the toroidal symmetry between mean values of ELM energy detected at two different locations for a given temporal phase of the discharge - $R = \left\langle E_{dep}^{\varphi=60} \right\rangle / \left\langle E_{dep}^{\varphi=165} \right\rangle$. Here $\left\langle E_{dep} \right\rangle$ is defined as a mean energy averaged over time deposited to the inner leg. As expected from previous work [3,11] without the RMP this ratio oscillates around a value of $R = 1$ independent of q_{95}. Applying magnetic perturbations introduces asymmetries of up to 20% between the radially integrated ELM energy at the two toroidal locations. With the RMP applied the value of R changes with safety factor as well, but not as regular as in the non-RMP case. The asymmetry is most likely caused by the 3D structure of the stochastic boundary, which is very sensitive to the safety factor profile. One of the effects of changing q_{95} is modification of the lobe positions on a target [15]. This is most likely the explanation of the variation of toroidal asymmetry with safety factor during the RMP. Please note that the changes in the asymmetries with q_{95} are larger at higher heating power, which again suggests better coupling of perturbation fields with plasma equilibrium.

As seen above on DIII-D, similar to other experiments, the ensemble average radially integrated power loads due to type-I ELMs are toroidally symmetric with variability of about 50%. This can be understood if we compare the dynamics of heat load patterns as measured by two cameras during an ELM. Figure 3(a) presents the heat flux density during the same event measured by the two cameras (left graph – $\varphi = 165°$, right one – $\varphi = 60°$). Although we observe that the rise time of power flux and decay are of the same order, the evolution and structures are rather different at two toroidal locations. Applying

5 kA of I-coil current creates a stochastic boundary in the plasma edge and the specific structure of the manifolds intersecting the target plates. In the discharge #139743 with q_{95} = 3.5 this produces small mitigated ELMs depositing 3 kJ on average to the divertor. As can be seen in Figs. 3(b)-3(c) these ELMs all have very similar structure, which follows the inter-ELM stochastic footprints. Smaller ELMs with $E_{dep} \leq 3$ kJ form two substructures on the target [Fig. 3(b)], whereas those with higher E_{dep} [Fig. 3(c)] create a third lobe at about 70-80 mm from the separatrix. Consistent with findings in [9] larger ELMs expel enough energy through the SOL in order to fill that outer lobe.

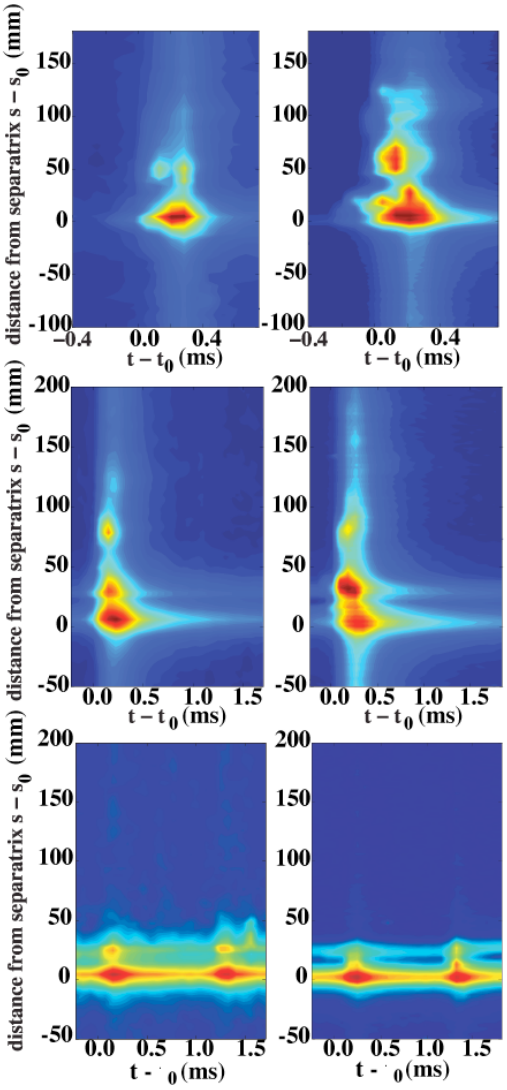

Fig. 3: An example of type-I ELM evolution (#139743, q_{95} = 3.5) on divertor surface measured by two different cameras (left SBFP at 165 deg, right FLIR at 60 deg) during no RMP phase, P_{tot} = 6 MW (a) and with RMP applied and also P_{tot} = 6 MW (b)-(c), plotted vs time and distance from separatrix.

One of the important questions for ITER is whether use of RMPs can realize scenarios with small ELMs that do not exceed specific level of heat loads. PFC erosion considerations imply that the upper limit of energy deposited during an ELM in ITER must be less or equal to 0.3% of the energy stored in the plasma volume, which is a rather low value if we consider results of present machines operating in H-mode scenarios [3]. In Fig. 4 a probability distribution of ELMs with a given energy is shown. The data is collected from all four investigated discharges and the probability distribution is calculated separately for different phases of the discharge.

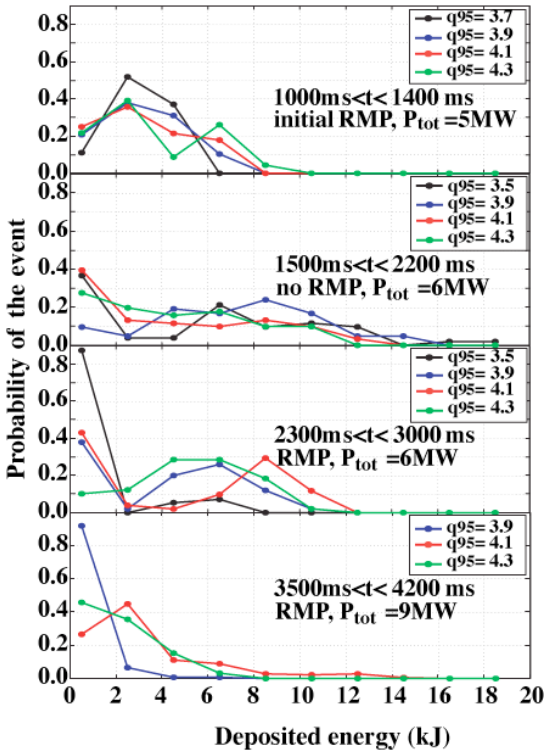

Fig. 4 Probability distribution of ELM energies as measured by the SBFP camera on inner divertor surface. Different colors of curves indicate different discharges (black – #139743, q_{95} = 3.5; blue – #139745, q_{95} = 3.9; red – #139747, q_{95} = 4.1, green – #139748).

1. In the initial phase (topmost graph), there is very weak effect of the perturbation fields on ELMs. All distributions for different values of q_{95} have rather similar shape with maximum population between 2 and 4 kJ. In the case of q_{95} = 3.7, black curve, there are no ELMs larger than 7 kJ in contrast to other discharges.
2. A second graph presents data for the very weak RMP phase of the discharge. Here we observe a rather wide spectrum of ELMs having different energies with a few cases of ELMs even with energy between 18 and 20 kJ. As expected those curves do not show any clear dependence on safety factor profile.

3. Applying the RMP at t = 2200 ms clearly changes distribution of ELM energies by shifting ELM energies towards lower values below 2 kJ. There are two subpopulations to be found in the graph with a border at about 3 kJ. The most optimal case is reached at q_{95} = 3.5, in which almost 90% of all events fall into energy range 0–3 kJ and few ELMs having energies of order of 4-8 kJ. At higher q_{95} the number of smaller ELMs is reduced. Please note that the distributions at q_{95} = 3.9 and 4.3 are rather similar, which was also true for values of R in Fig. 3. This suggests that, similar to the effect of magnetic perturbation on the plasma pressure profile [20] also mitigation of ELMs by RMP has more than one resonant window.
4. Increasing the heating power to 9 MW, as expected from results discussed above improves the mitigation effect. All distributions have most of the events below 5 kJ. In the case of q_{95} = 3.9 we did not detect single ELM with energy above 5 kJ. Also there a case at q_{95} = 4.3 (green curve) seems to have a stronger influence of RMP on ELMs than the one at q_{95} = 4.1 (red curve). In the latter one there are still some events with $E_{dep} < 8$ kJ. Please note, that both cases without RMP are very similar.

IV. SUMMARY

In this paper we have discussed scenarios of H-mode plasmas with RMPs, in which the ELMs are mitigated rather than fully suppressed. With proper value of safety factor a discharge was achieved in which all ELMs deposit on average about 3 kJ to the lower divertor. The probability distribution made for ELMs in the inner leg shows that about 90% of events deposit less than 3 kJ at the location of the SBFP camera (i.e. at $\varphi = 165°$) and no ELM depositing more than 5 kJ there. This is very promising for ITER because small, well-controlled ELMs during the discharge could help to exhaust impurities from the plasma volume and might not reduce the lifetime and the durability of divertor surface. The effect of RMP on ELM behavior seems to have multiple resonant windows with the optimum reached at $q_{95} \approx 3.9$ and $P_{tot} = 9$ MW, when very strong ELM suppression is reached when H98 reaches pre-RMP value of 1.2. Worth noting is that at higher heating power the response to magnetic perturbation is stronger, which is consistent with the findings in [21].

Without the RMP ELMs deposit the same energy radially integrated on average at both toroidal locations being observed, but individual events show a rather different structure and evolution of heat flux patterns. Applying the RMP forces ELMs to deposit power along channels defined by the manifolds of the stochastic boundary which introduces toroidal asymmetries, but significantly reduces ELM energies and their wetted area.

REFERENCES

[1] F. Wagner, *et al.,* Plasma Phys. Control. Fusion **48**, A217-A239 (2006).

[2] H. Zohm, Plasma Phys. Control. Fusion **38**, 105-128 (1996).

[3] A. Loarte, *et al.*, Plasma Phys. Control. Fusion **45**, 1549-1569 (2003).

[4] A. Kirk, *et al.*, Plasma Phys. and Control. Fusion **47**, 315-333 (2005).

[5] A. Herrmann, J. Nucl. Mater. **363-365**, 528-533 (2007).

[6] A. Kirk, *et al.*, Phys. Rev. Lett. **96**, 185001-4 (2006).

[7] M. Jakubowski, *et al.*, J. Nucl. Mater. **390-391**, 781-784 (2009).

[8] T. Eich, A. Herrmann, J. Neuhauser, Phys. Rev. Lett. **91**, 195003 (2003).

[9] M. Jakubowski, *et al.*, Nuclear Fusion **49**, 095013 (2009).

[10] G. Federici, *et al.*, Nucl. Fusion **41**, 1967-2137 (2001).

[11] A. Herrmann, Plasma Phys. Control. Fusion **44**, 897-917 (2002).

[12] T. Evans, *et al.*, J. Nucl. Mater. **390-391**, 789-792 (2009).

[13] T. Evans, *et al.*, Nucl, Fusion **48**, 024002 (2008).

[14] T.E. Evans, *et al.*, Phys. Rev. Lett. **92**, 235003 (2004).

[15] O. Schmitz, *et al.*, Plasma Phys. Control. Fusion **50**, 124029 (2008).

[16] T.E. Evans, *et al.*, Phys. Plasmas **9**, 4957-4967 (2002).

[17] A. Herrmann, *et al.*, Plasma Phys. Control. Fusion **37**, 17-29 (1995).

[18] T. Eich, *et al.*, Plasma Phys. Control. Fusion **49**, 573-604 (2007).

[19] R. Fitzpatrick, Phys. Plasmas **10**, 1782 (2003).

[20] O. Schmitz, *et al.*, Phys. Rev. Lett. **103**, 165005 (2009).

[21] D. Orlov, *et al.*, Nucl. Fusion **50**, 034010 (2010).

ACKNOWLEDGMENT

This work was supported in part by the U.S. Department of Energy under DE-FC02-04ER54698, DE-AC52-07NA27344, DE-AC05-00OR22725, DE-FG02-07ER54917, DE-FG03-08ER54984, and DE-AC04-94AL85000.